

Measurements of jet and photon production properties in pp collisions with the ATLAS detector

Mikhail Demichev*

*Joint Institute for Nuclear Research, 141980, Dubna, Moscow Region, Russian Federation
Moscow Institute of Physics and Technology, 141700, Dolgoprudny, Moscow Region, Russia
E-mail: mikhail@cern.ch*

The results of measurements of jet and photon production properties in pp collisions with the ATLAS detector are presented including direct photon, photon+jet, diphoton cross section measurement, dijet cross section and jet veto correlations.

*XXII International Baldin Seminar on High Energy Physics Problems,
15-20 September 2014
JINR, Dubna, Russia*

*Speaker.

1. Introduction

Prompt photons are all kind of photons coming from proton-proton collisions at LHC 1a, 1b excluding photons from decay of secondary particles 1c.

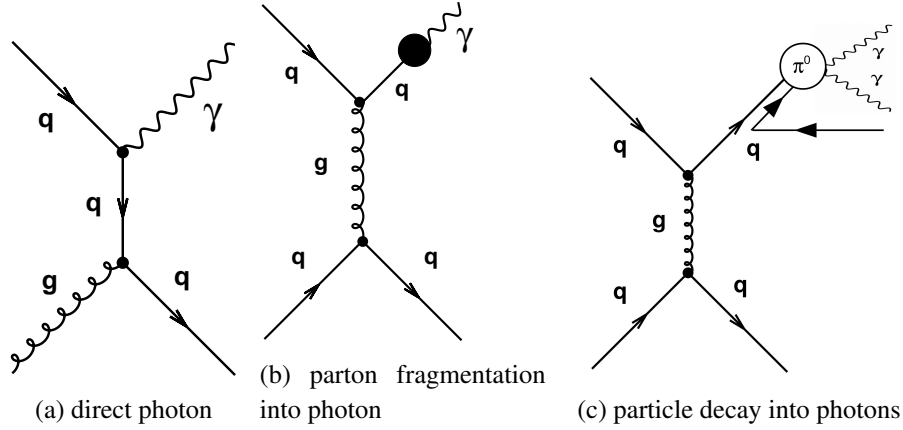
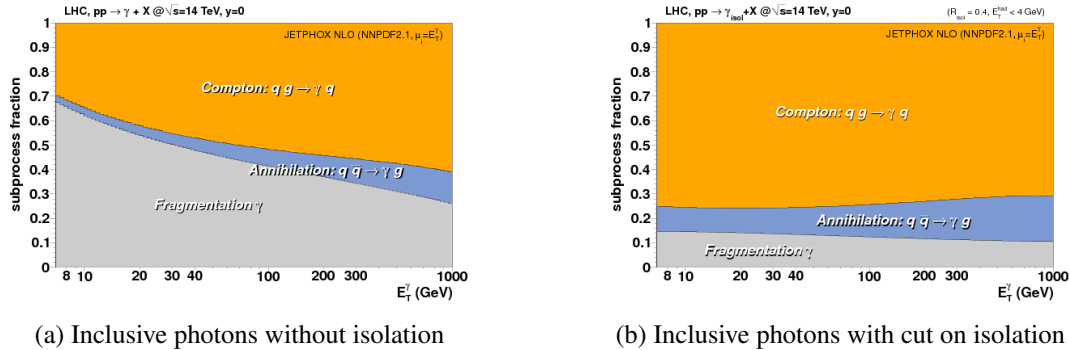


Figure 1: photon production

To distinguish prompt photons from decay photons an selection on photon isolation energy is used. This important experimental quantity will be described later in this paper. Also isolation criteria reduces contribution of fragmentation photons 2.



(a) Inclusive photons without isolation (b) Inclusive photons with cut on isolation

Figure 2: Impact of isolation on the components ratio of inclusive photon production

Prompt isolated photons can be used as probe for PDF gluon density studies [1]. A combined measurement of ATLAS and CMS using $\sqrt{s} = 7TeV, L = 37pb^{-1}$ 2010 data constrain PDF in $x \approx 0.002 - 0.05$ at scales $Q^2 = 10 - 10^4 GeV^2$ 3.

With photon and jet we can study the basic predictions of pQCD measuring the scattering angle between photon and jet $\cos \theta^{\gamma j} = \tanh(y^\gamma - y^j)$. For quark exchange it is $\approx (1 - |\cos \theta^{\gamma j}|)^{-1}$ while for gluon exchange $\approx (1 - |\cos \theta^{\gamma j}|)^{-2}$.

2. Photon identification and isolation at ATLAS

Photon identification is used to distinguish a photon from an electron and both of them from

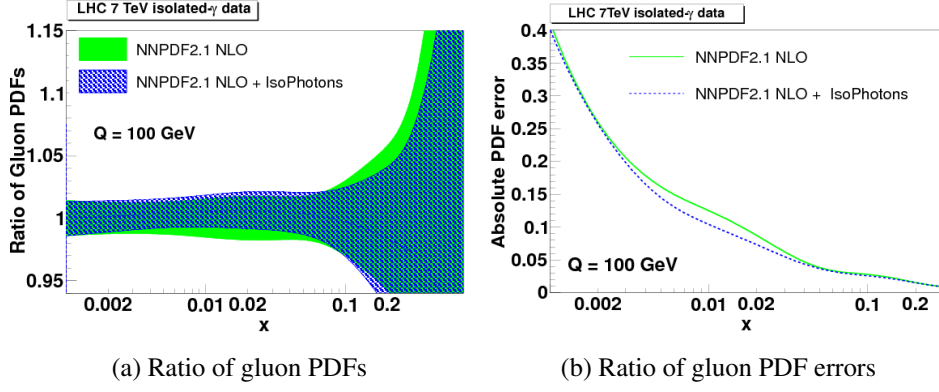


Figure 3: Impact of combined LHC 7 TeV isolated photon measurements on gluon PDF and its errors

a jet. In ATLAS is based upon likelihood function discrimination built with several shower shape variables which are ratios of energy deposit in different layers and segments of electromagnetic and hadronic calorimeters. Tight ID is the discrimination criteria based on nine different shower shapes which gives fine degree of probability that our reconstructed object is a photon. Loose ID criteria is based on subset of five shower shapes and is used to control background contamination of tight photons. Technically it is the fine segmentation of calorimeter first layer 4 ($\Delta\eta_x\Delta\phi = 0.003x0.025$) which gives the possibility for discrimination between prompt photons and π_0, η decay photons

Isolation energy is sum of clusters energy from both hadronic and EM calorimeters inside the standard jet cone of $\Delta R = 0.4$ but excluding photon core of 5×7 cells in 2nd layer of EM calorimeter.

Tight isolated 5 reconstructed photons consist mostly of prompt photons with reduced contribution of fragmentation photons and negligible contribution of background from decay photons and hadronic jets.

3. Isolated prompt photon production at 7 TeV [2]

Inclusive isolated photons $p + p \rightarrow \gamma + X$, $\sqrt{s} = 7\text{TeV}$, $L = 4.7\text{fb}^{-1}$.

- $E_T^\gamma > 100\text{GeV}$, $\eta_\gamma < 2.37$, excluding gap $1.37 < \eta_\gamma < 1.52$
- tight, isolated photons $E_T^{\text{iso}} < 7\text{GeV}$
- 2D-sideband data-driven method of residual background subtraction is used
- photon distributions are corrected for detector effects
- The NLO calculations agree with data up to 1 TeV within theoretical uncertainty
- Pythia describes the data fairly well
- HERWIG underestimates fragmentation at low E_T by $\approx 10\%$

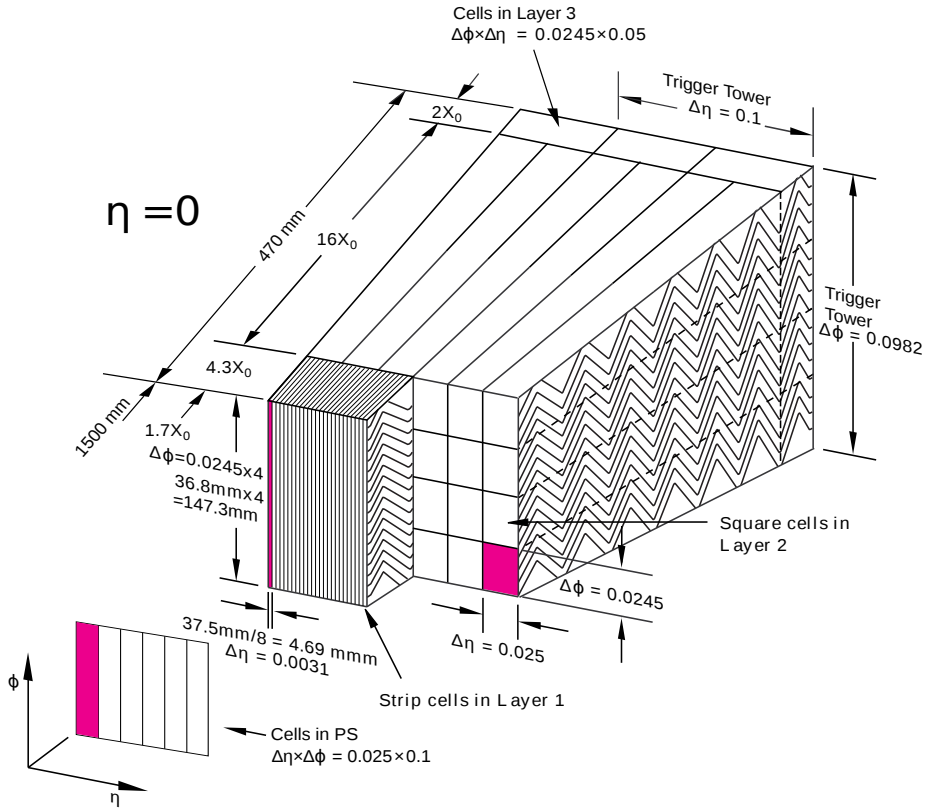


Figure 4: Segmentation of ATLAS electromagnetic calorimeter

4. Dynamics of photon + jet cross production in at 7 TeV

Dynamics of isolated-photon + jet production in proton-proton collisions at 7 TeV with integrated luminosity $L = 37 \text{ pb}^{-1}$ using 2010 data taking period has been measured [3].

Photon and jet selection:

- $p + p \rightarrow \gamma + \text{jet} + X, \sqrt{s} = 7 \text{ TeV}, L = 37 \text{ pb}^{-1}$
- photon: $E_T^\gamma > 45 \text{ GeV}, \eta_\gamma < 2.37$, excluding gap $1.37 < \eta_\gamma < 1.52$, tight, $E_T^{\text{iso}} < 3 \text{ GeV}$
- jet: $p_T^{\text{jet}} > 40 \text{ GeV}, \eta_{\text{jet}} < 2.37$, discarding jets that overlap with photon in $\Delta R = 1$

Measured cross section of photon + jet as functions of photon E_T and jet p_T is shown on figure 7.

Good description by NLO pQCD for $d\sigma/dE_T^\gamma$ and $d\sigma/dp_T^{\text{jet}}$. Very close predictions for CTEQ6.6 and CT10 PDFs, MSTW2008nlo is 5% higher than data. Experimental uncertainties $\approx 10\%$ are dominated by jet energy scale. Theoretical uncertainties $\approx 10\%$ are dominated by terms beyond NLO.

To measure angular dependence 8 additional phase space constraints are provided

$$|\eta^\gamma + \eta^{\text{jet}}| < 2.37, |\cos \theta^{\gamma j}| < 0.83, m^{\gamma j} > 161 \text{ GeV}$$

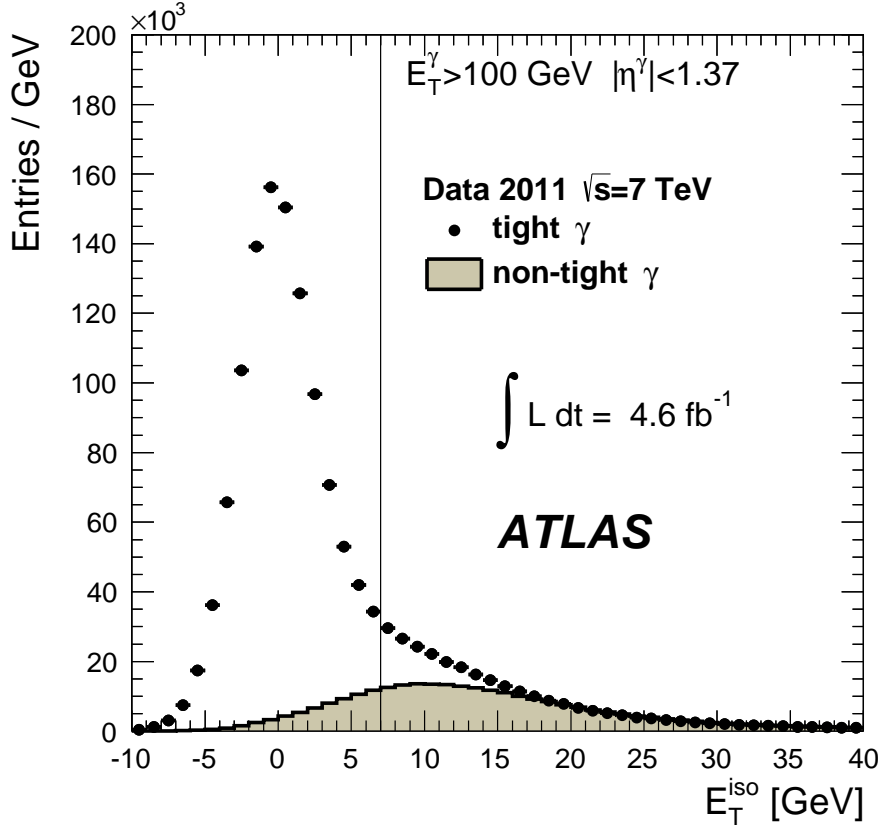


Figure 5: Isolation energy profiles for photons identified as tight and non-tight

to ensure that $m^{\gamma j}$ and $\cos \theta^{\gamma j}$ distributions are not distorted by selection cuts on photon and jet. Direct photons [1a](#) produced in compton-like quark-gluon scattering with quark exchange give $\approx (1 - |\cos \theta^{\gamma j}|)^{-1}$ angular dependence. The fragmentation photon and jet produced when a two quarks are scattered via gluon exchange [1b](#) and later one of the quarks transfers most of its energy into collinear photon with a so called fragmentation function. So the angular distribution of fragmentation photon + jet will be the same as for di-jet events $\approx (1 - |\cos \theta^{\gamma j}|)^{-2}$.

NLO pQCD (JetFox) gives good description for $d\sigma/dm^{\gamma j}$ and $d\sigma/d\cos \theta^{\gamma j}$. The shape of measured angular distribution [8c](#) is closer to that of *direct* photon than to *fragmentation* one. The fit to can be used to determine the ratio of direct/fragmentation components.

5. isolated diphoton cross section measurements at 7 TeV

Diphoton measurements [\[4\]](#), $L = 4.9 fb^{-1}$

- understanding irreducible background for $H \rightarrow \gamma\gamma$ and new physics
- event selection:
 - leading photon $E_T^\gamma > 25 GeV$, subleading photon $E_T^\gamma > 22 GeV$

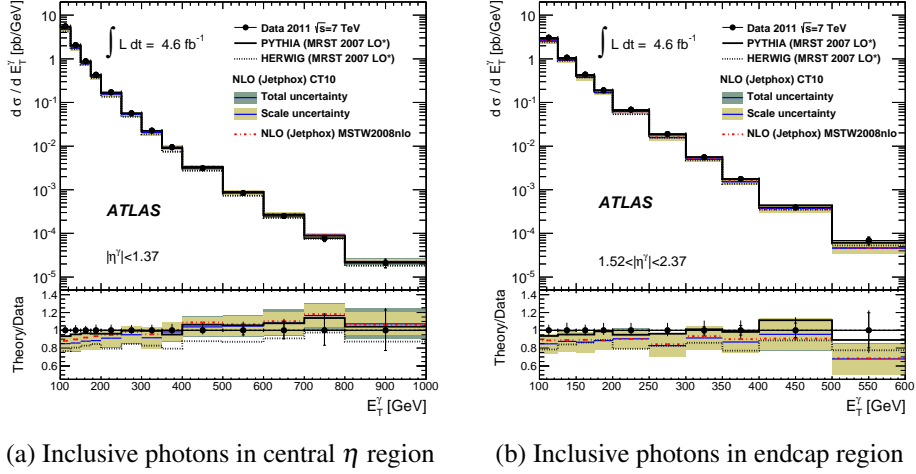
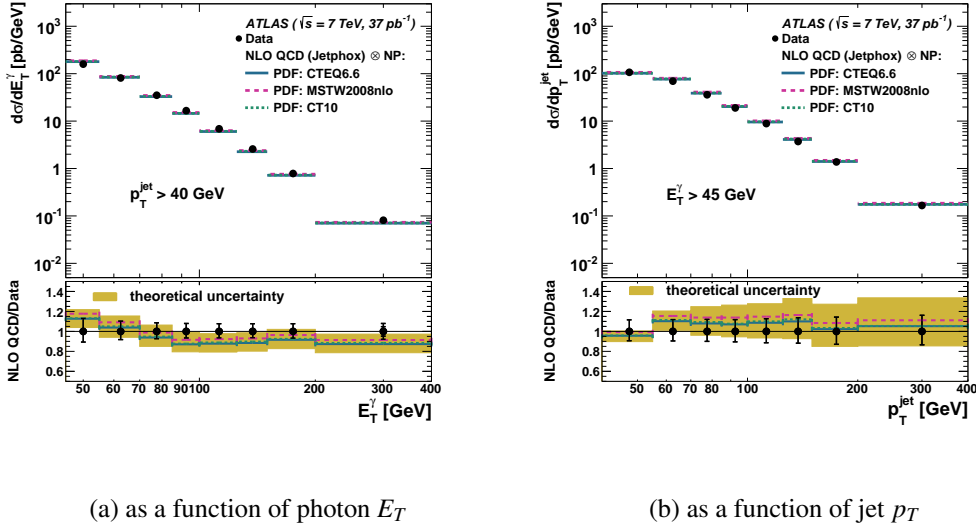
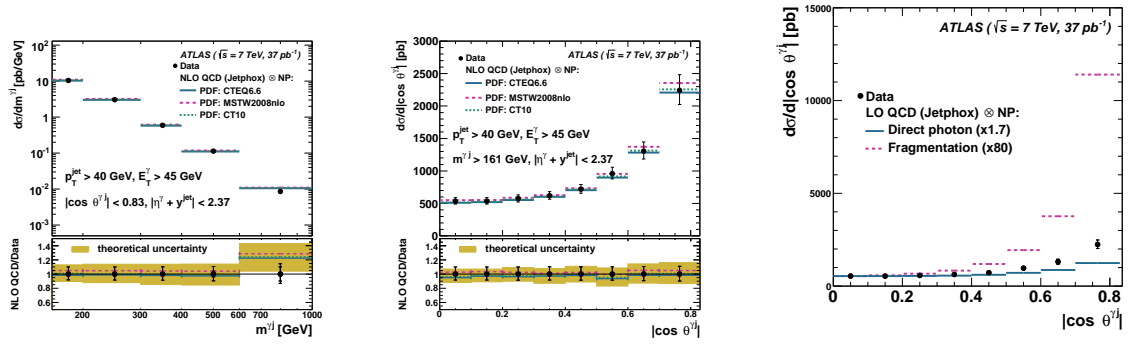

 Figure 6: Measured cross section as function of photon E_T


Figure 7: cross section of photon + jet for 7 TeV data taking

- $|\eta_\gamma| < 2.37$ excluding the gap region $1.37 < |\eta_\gamma| < 1.52$
- isolation requirement $E_T^{iso} < 4\text{GeV}$, photon separation $\Delta R_{\gamma\gamma} > 0.4$
- two alternative methods applied to subtract the jet background of γj , $j\gamma$, jj events
 - 2x2D-sideband method
 - 2D-template fit method for isolation distribution with applied leakage corrections
 - the difference of $\approx 1.5\%$ is included as systematic uncertainty for isolation
- corrected for electron (misidentified as gamma) background from Z and W decays
- final measurements are corrected for detector and resolution effects



(a) as a function of invariant mass of photon and jet (b) as a function of scattering angle (c) shape comparison of data with direct and fragmentation components

Figure 8: cross section of photon + jet for 7 TeV, with additional phase space constraints

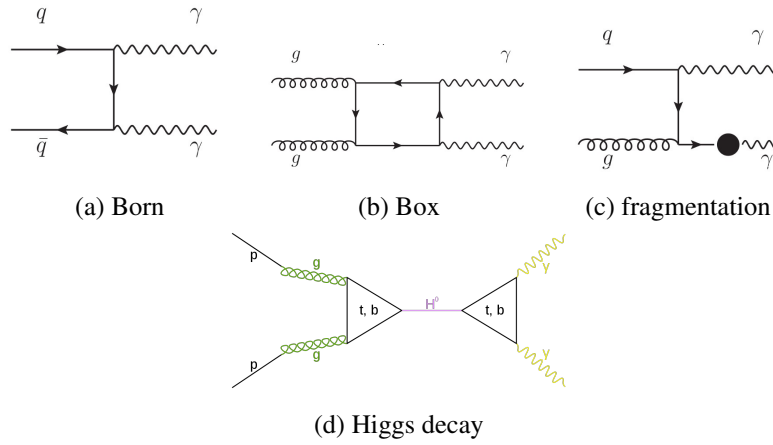


Figure 9: Important processes with dithotons in final state

Diphoton $\frac{d\sigma}{dm_{\gamma\gamma}}$ [4], $L = 4.9 fb^{-1}$

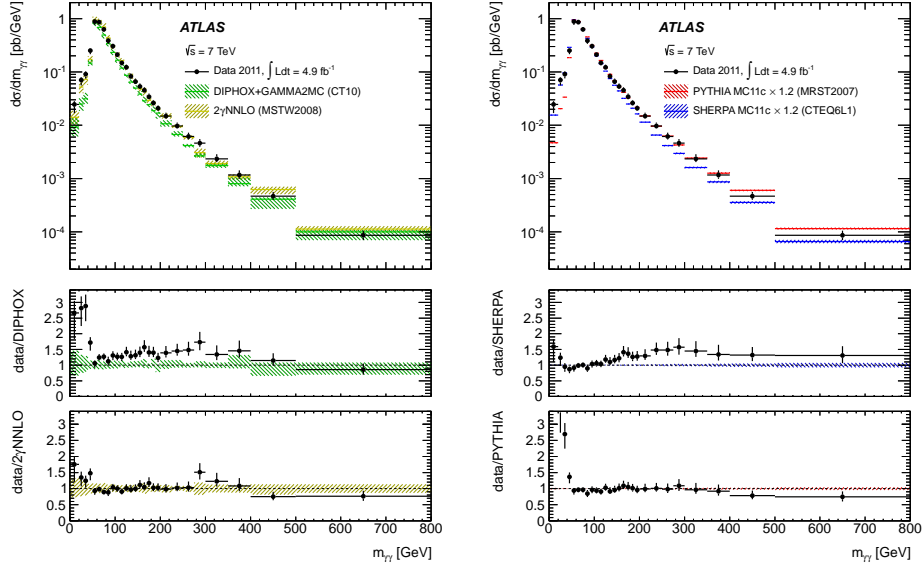
- overall good agreement with $2\gamma NNLO$, DIPHOX is missing NNLO contribution
- low $m_{\gamma\gamma}$: SHERPA (includes $2 \rightarrow 4$ processes) is better than Pythia; intermediate $m_{\gamma\gamma}$: better description by Pythia

Diphoton $\frac{d\sigma}{dp_{T,\gamma\gamma}}$ [4], $L = 4.9 fb^{-1}$

- DIPHOX and $2\gamma NNLO$ fail at low p_T due to initial state soft-gluon radiation divergency
- good agreement with SHERPA and at high p_T with $2\gamma NNLO$

Diphoton $\frac{d\sigma}{d\Delta\phi_{\gamma\gamma}}$ [4], $L = 4.9 fb^{-1}$

- good agreement with SHERPA and $2\gamma NNLO$



(a) Data compared with NNLO calculations (b) Data compared with LO predictions (scaled)

Figure 10: Cross section as a function of diphoton invariant mass

- high $\Delta\phi_{\gamma\gamma}$ region sensitive to initial state soft-gluon radiation: DIPHGX and $2\gamma NNLO$ overestimate data

Diphoton $\frac{d\sigma}{d\cos\theta_{\gamma\gamma}^*}$ [4], $L = 4.9 fb^{-1}$

- overall good agreement except for large $\cos\theta_{\gamma\gamma}^*$ dominated by fragmentation

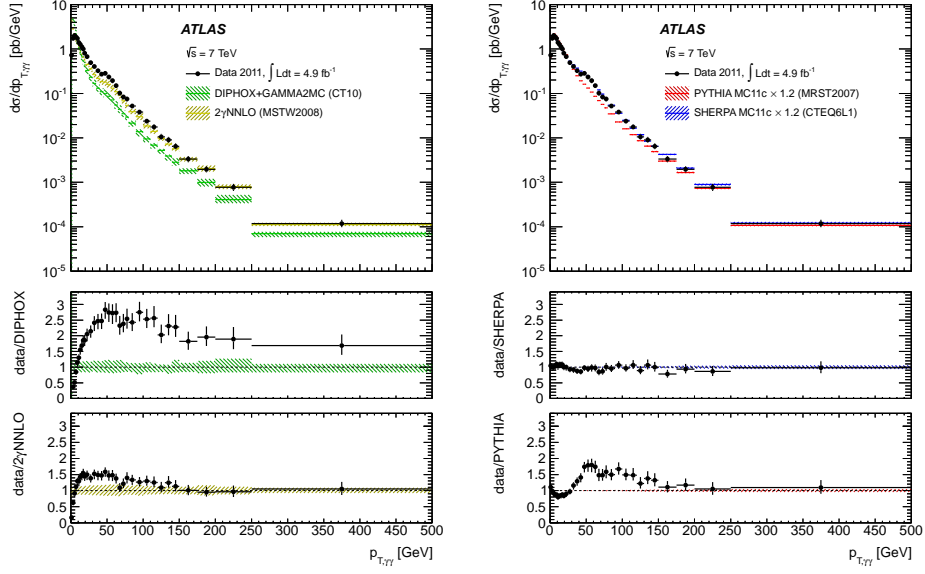
6. dijet production at 7 TeV

Dijet cross section [5], $\sqrt{s} = 7TeV, L = 4.5 fb^{-1}$. QCD processes are dominant at hadron colliders so dijet measurements are the most abundant from all the hard scattering processes and give enough statistics to probe highest energy transfers up to 5 TeV in m_{12} for $\sqrt{s} = 7TeV$. From dijet measurements experimental constraints on proton PDFs can also be derived (especially for gluon density at high x). Multijet topologies are interesting because they are background to the expected new physics.

Di-jet selection:

- anti- k_r jet algorithm
- all measurements done for two cone sizes $\Delta R = 0.4$ and $\Delta R = 0.6$
- leading jet $p_T > 100GeV$, subleading $p_T > 50GeV$, $|y_{jet}| < 3$

Doubly differential cross section of di-jet production is measured [14] as function of m_{12} for several $y^* = |y_1 - y_2|$ bins. The measurement shows good agreement between data and MC and is



(a) Data compared with NNLO calculations

(b) Data compared with LO predictions (scaled)

Figure 11: Cross section as a function of average transverse momentum of 2 photons $P_{T,\gamma\gamma}$

tested for stability against pile-up. Experimental uncertainties 10% for low m_{12} , up to 25% at high m_{12} , out of them jet-energy calibration gives $\approx 1\% - 2\%$.

CT10 describes well the measurements for both jet radii. HERAPDF1.5 has disagreement at some m_{12} at certain y^* . Using the p-value to compare the degree of agreement between data and NLO calculations with different PDFs.

MSTW2008, NNPDF2.3 describe well the measurements for both jet radii. ABM11 has disagreement at some regions of m_{12} . This measurement provides experimental input for further constraints on PDFs.

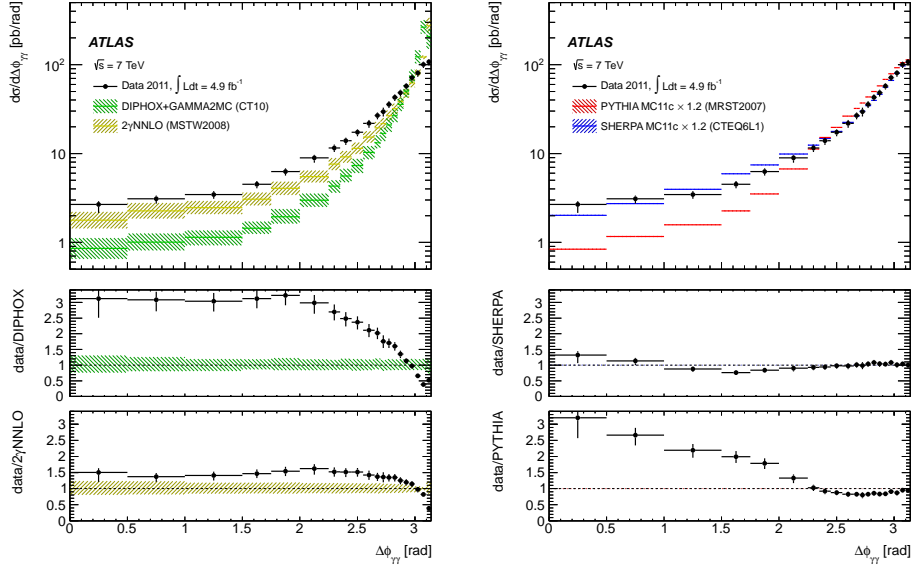
7. Jet asimuthal decorrelation studies at 7 TeV

Jet asimuthal decorrelations [6], $\sqrt{s} = 7TeV, L = 36.1pb^{-1}$ and $L = 4.5fb^{-1}$. Jet veto for dijet events 17 means that for a given jet rapidity separation there is no other jet with energy greater than given value between the selected two jets.

Fixed order QCD predictions expect to perform poorly when higher order terms are important:

- large rapidity separation Δy
- when jet veto above Q_0 applied

To combine that two cases into a single variable the gap fraction $f(Q_0) = \frac{\sigma_{jj}(Q_0)}{\sigma_{jj}}$ is measured 18. It is the ratio of numbers of dijet events selected using the same selection cuts but with jet veto applied and without any veto. Gap fraction distribution is sensitive to BFKL at large Δy and when



(a) Data compared with NNLO calculations (b) Data compared with LO predictions (scaled)

Figure 12: Cross section as a function of transverse angular difference of 2 photons

average transverse momentum of the jets $\overline{p_T} \gg Q_0$ wide-angle soft gluon radiation becomes important. Improved results are expected if HO are resummed in terms of $\ln(1/x)$ (BFKL approach) or in terms of $\ln(Q^2)$ (DGLAP approach).

Jet selection: jets are reconstructed with anti- k_t jet $\Delta R = 0.6$ algorithm.

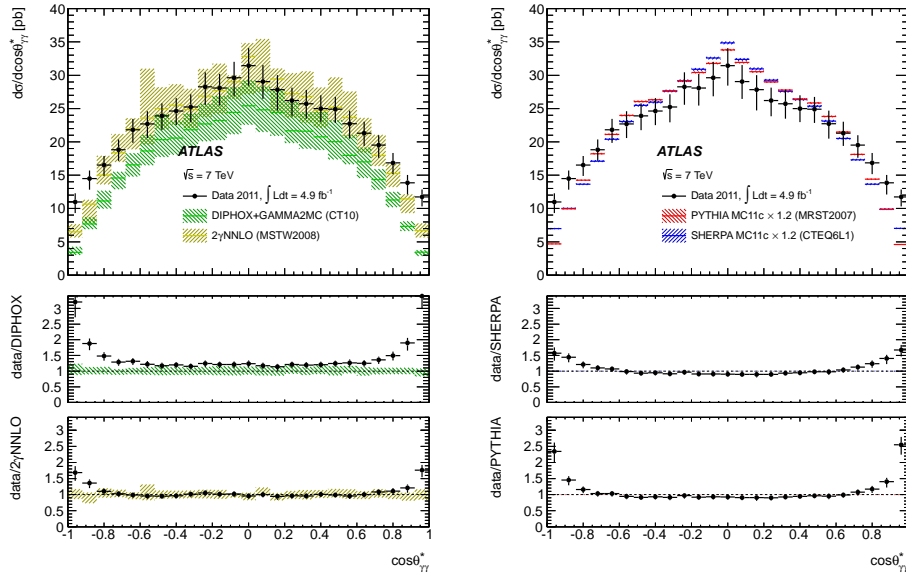
- Leading jet $p_T^{jet} > 60 GeV$, sub-leading jet $p_T^{jet} > 50 GeV$
- 2010: $|y_{jet}| < 4.4$, gap fraction with veto scale $Q_0 = 20 GeV$
- 2011: $|y_{jet}| < 2.4$, gap fraction with veto scale $Q_0 = 30 GeV$

For 2011 data a somewhat higher veto energy is used.

HEJ+ARIADNE describes the gap fraction for low and medium Δy and $\overline{p_T}$. POWHEG describes the gap fraction for low Δy and for all $\overline{p_T}$. The HEJ/HEJ+ARIADNE follow BFKL approach and POWHEG+PYTHIA/HERWIG follow DGLAP approach.

8. Summary

- Inclusive photon production
 - tests of pQCD in a clean environment
 - sensitivity to the gluon component of proton PDF
- Photon + jet production
 - tests of color dynamics with an accuracy of $\approx 10\%$



(a) Data compared with NNLO calculations (b) Data compared with LO predictions (scaled)

Figure 13: Cross section as a function of scattering angle between 2 photons

- dynamics of photon+jet production has good description at the order of $O(\alpha\alpha_s^2)$
- Diphoton production
 - irreducible background to $H \rightarrow \gamma\gamma$
 - improved calculations are required to provide a better description at high orders
- Dijet production with and without veto
 - good description of dijet data by pQCD at the highest energy transfer
 - jet-veto measurements have no consistent description over the full phase space with DGLAP and BFKL approaches
- coming soon: inclusive jets and three-jet measurements at 7 TeV

References

- [1] D.d'Enteria, J.Roho, *Quantitative constraints on the gluon distribution function in the proton from collider isolated-photon data*, *Nucl.Phys.B* **860**,311-338, (2012)
- [2] ATLAS Collaboration, *Measurement of the inclusive isolated prompt photon cross section in pp collisions at $\sqrt{s} = 7\text{TeV}$ with the ATLAS detector using 4.6fb^{-1}* , *Phys.Rev.D* **89**, 052004, (2014)
- [3] ATLAS Collaboration, *Dynamics of isolated-photon and jet production in pp collisions at $\sqrt{s} = 7\text{TeV}$ with the ATLAS detector*, *Nucl.Phys.B* **875**,483-535, (2013)
- [4] ATLAS Collaboration, *Measurement of isolated-photon pair production in pp collisions at $\sqrt{s} = 7\text{TeV}$ with the ATLAS detector*, *JHEP* **01**, 086 (2013)

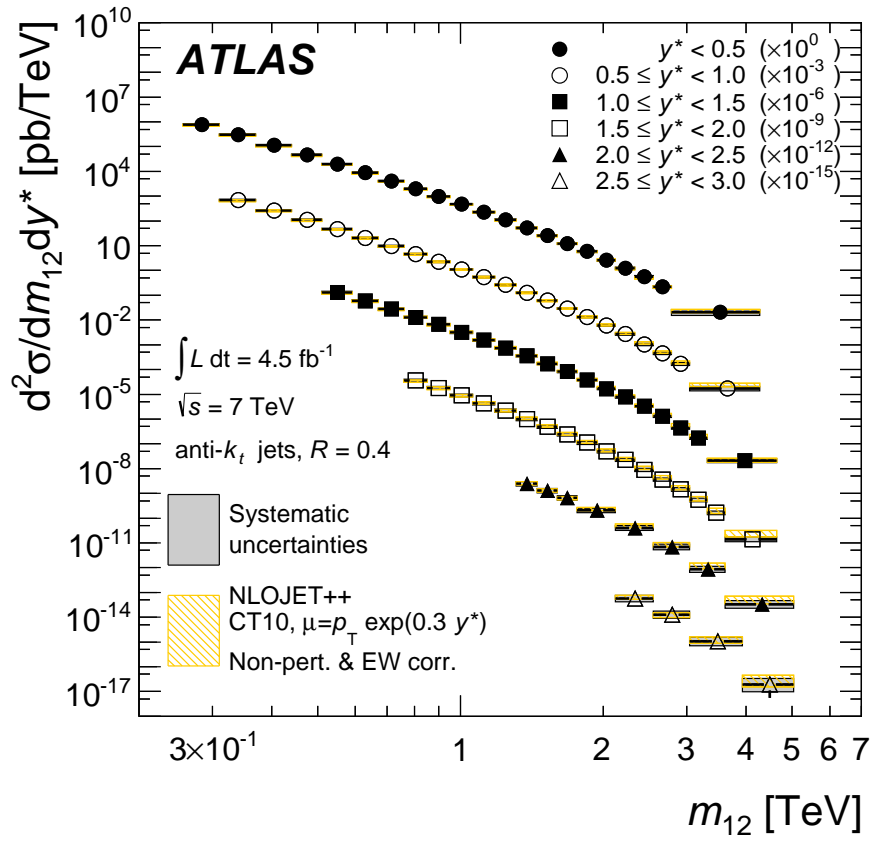


Figure 14: Dijet production cross section as a function of invariant mass and rapidity

- [5] ATLAS Collaboration, *Measurement of dijet cross sections in pp collisions at 7TeV centre-of-mass energy using the ATLAS detector*, *JHEP* **05**, 059 (2014)
- [6] ATLAS Collaboration, *Measurements of jet vetoes and azimuthal decorrelations in dijet events produced in pp collisions at sqrt(s) = 7TeV using the ATLAS detector*, submitted to EPJC

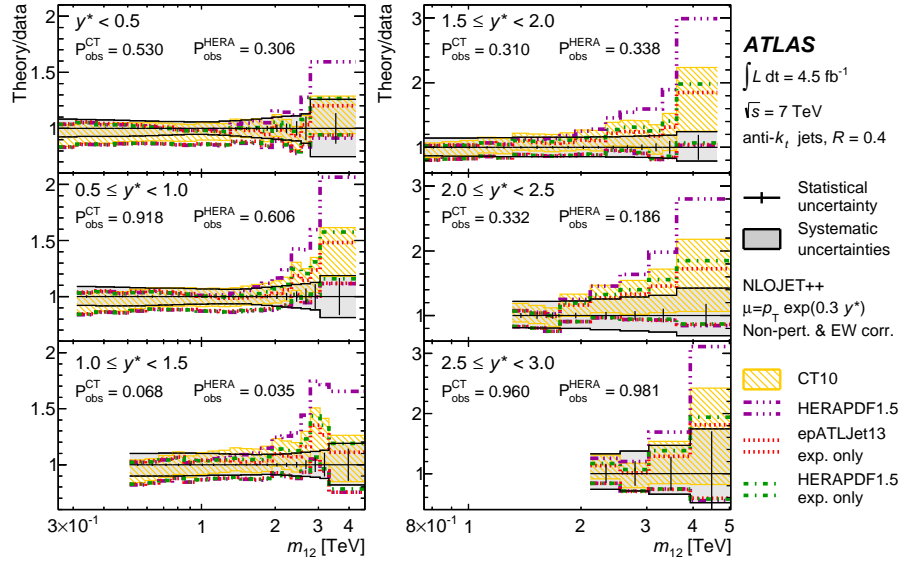


Figure 15: Ratio of NLO QCD predictions of NLOJet++ to the unfolded measurements of dijet cross section as a function of y^* for jet radius $R = 0.4$ with PDF sets used: CT10, HERAPDF 1.5 and epATLJet13

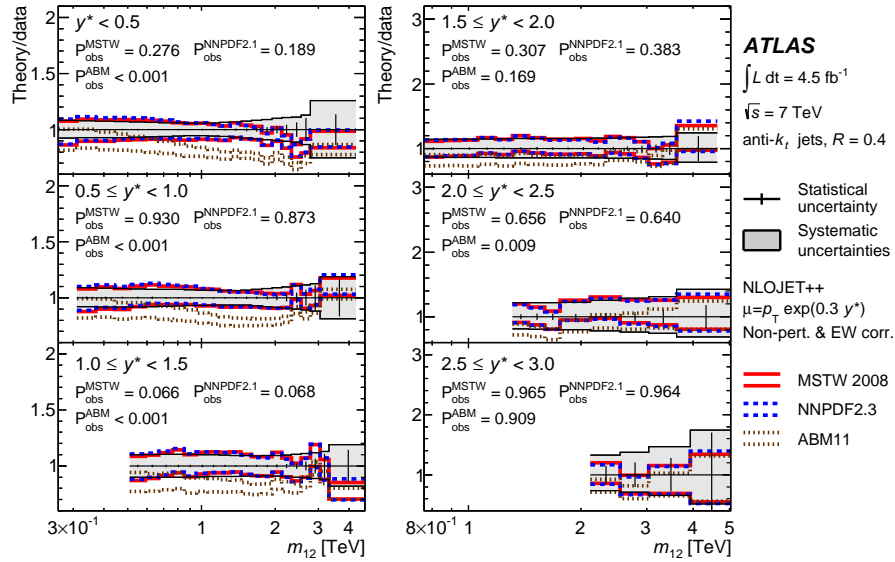


Figure 16: Ratio of NLO QCD predictions of NLOJet++ to the unfolded measurements of dijet cross section as a function of y^* for jet radius $R = 0.4$ with PDF sets used: MSTW2008, NNPDF2.3 and ABM11

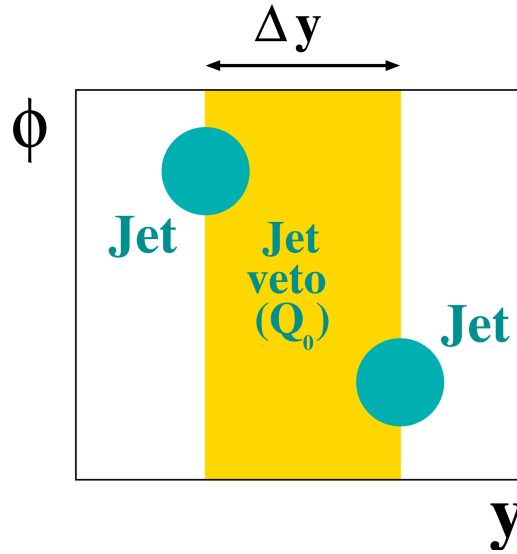
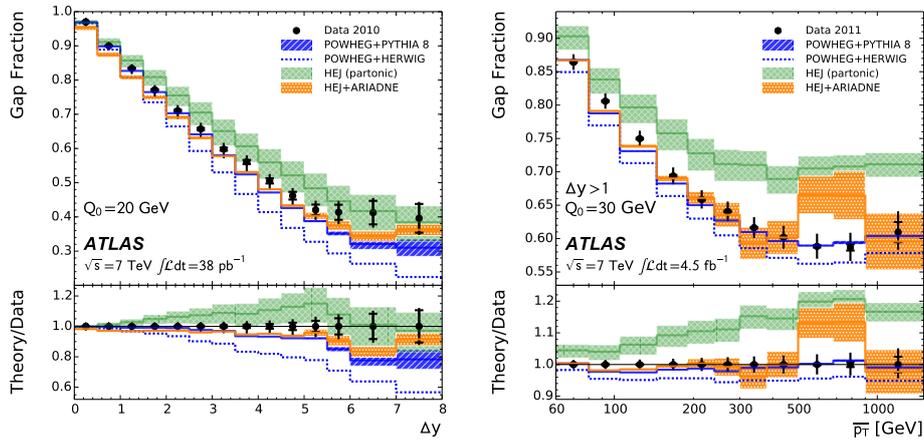


Figure 17: Jet veto: No extra jets with $p_T > Q_0$ between j_1 and j_2



(a) as a function of rapidity difference for 2010 data

(b) as a function of average dijet transverse momentum for 2011 data

Figure 18: Gap fraction